Soft Matter

Accepted Manuscript

Journal Name

ARTICLE TYPE

Short-time dynamics in dispersions with competing short-range attraction and long-range repulsion

Jonas Riest* and Gerhard Nägele

Dynamic clustering of globular Brownian particles in dispersions exhibiting competing short-range attraction and long-range repulsion (SALR) such as low-salinity protein solutions has gained a lot of interest over the past years. While the structure of the various cluster phases has been intensely explored, little is known about the dynamics in SALR systems. We present the first systematic theoretical study of short-time diffusion and rheological transport properties of two-Yukawa potential SALR systems in the single-particle dominated dispersed-fluid phase, using semi-analytic methods where the salient hydrodynamic interactions are accounted for. We show that the dynamics has unusual features compared to reference systems with pure repulsion or attraction. Results are discussed for the hydrodynamic function characterizing short-time diffusion that reveals an intermediate-range-order (cluster) peak, self-diffusion and sedimentation coefficients, and high-frequency viscosity. As important applications, we discuss the applicability of two generalized Stokes-Einstein relations, and assess the wavenumber range required for the determination of self-diffusion in a dynamic scattering experiment.

1 Introduction

Brownian particle dispersions with short-range attraction (SA) and long-range repulsion (LR) such as low-salinity lysozyme protein solutions, and suspensions of micron-sized charged colloidal particles with added depletant , have been intensely studied over the past years [1–8]. SALR protein systems are particularly interesting, since the clustering of proteins can result in severe diseases such as Alzheimer and Parkinson [9,10]. Stradner *et al.* [1] observed experimentally a small-wavenumber peak in the static structure factor, $S(q)$, at a wavenumber, q_c, distinctly smaller than the wavenumber, q_m, where the next-neighbor peak of individual particles of height $S(q_m)$ is located. They attributed the structure factor peak at q_c to the formation of particle clusters. A cluster peak of $S(q)$ is indeed observed for the mesoscopically inhomogeneous cluster-fluid phase of reversibly formed fluid-like clusters in equilibrium with individually dispersed particles (monomers) [2,5,7]. This phase is stabilized against macroscopic phase separation by the long-range repulsive interaction part which limits the mean cluster size and suppresses cluster-cluster aggregation.

Liu *et al.* [4,5] showed subsequently that a small-wavenumber peak at a wavenumber $q_c < q_m$ is indicative not only of the cluster-fluid phase. It is present, in particular, also in the so-called dispersed-fluid phase of SALR systems occurring for smaller con-

centrations and interaction strengths (i.e., larger reduced temperatures) where non-associated monomers are dominant, and where the $S(q_c)$-peak is indicative of intermediate-range microstructural ordering (IRO) arising from the competing SA and LR.

In the past few years, the microstructure and cluster states of the two-Yukawa [5,11] SALR potential model, and the generalized ($2\alpha^*$-α^*) Lennard-Jones (LJ) - Yukawa SALR potential for typical LJ power law exponents $\alpha^* \sim 90 - 100$ [6] have been intensely studied. Associated reduced temperature-concentration state diagrams [2,5,6] have been mapped out, and compared with experimental results in particular for zero-salt lysozyme solutions [2,5,7]. Depending on particle concentration, relative strength and range of the competing SA and LR potential parts determining the size and shape, and the lifetime of clusters, various dynamically arrested modulated phases have been found in addition to the dispersed-fluid and cluster-fluid phases, including cluster-percolated gels and glasses composed of clusters [2,3,5–7,11,12].

In comparison with the large body of work on the structure and phase behavior of SALR systems, little is known to date about their dynamic properties. This concerns in particular theoretical and simulation works on these systems that are challenging owing to the important influence of the hydrodynamic interactions (HIs). The HIs need to be accounted for in a realistic modeling. Rigid clusters behave hydrodynamically different from fluid-like ones since there is no hydrodynamic screening in the latter case. In earlier Brownian dynamics simulation calculations [2] of

Forschungszentrum Jülich GmbH, ICS-3 - Soft Condensed Matter, 52428 Jülich, Germany;
* E-mail: j.riest@fz-juelich.de

the dynamic structure factor, $S(q,t)$, and the wavenumber dependent short-time diffusion function, $D(q)$, based on the generalized Lennard-Jones-Yukawa SALR model, HIs were completely disregarded. Another complication in the theoretical description of cluster states arises from the presence of additional time and length scales associated with the distributions of cluster lifetimes, sizes and charges. This hampers a clear distinction between colloidal short-time and long-time regimes as it can be made for a homogeneous suspension of individually diffusing monodisperse particles. An interesting experimental observation pointing to these complications is the surprising observation that the short- and long-time self-diffusion coefficients for salt-free lysozyme solutions deduced from neutron spin echo (NSE) data share roughly the same concentration dependence[4].

In this work, we present a generic theoretical study of short-time diffusion and rheological transport properties of a SALR model system where the salient HIs are accounted for. We use an isotropic hard-core plus two-Yukawa pair potential, $V(r)$, consisting of soft SA and LR Yukawa potential parts respectively. This SALR potential is frequently used in studies of microstructural properties and phase behavior[3,8,13,14]. It describes phenomenologically the orientationally averaged short-range attraction of globular proteins, and the for low salinity systems long-ranged electric double layer repulsion originating from the protein charges and surface-released counterions.

The considered SALR systems are all in the homogeneous dispersed-fluid phase state where most particles diffuse individually. However, the tendency of clustering is noticeable also in this phase as hallmarked, e.g., by the occurrence of an IRO peak in $S(q)$ that grows with increasing α and ϕ as the transition line to the cluster-fluid phase is approached.

This transition line marks a microphase separation into clusters owing to the suppression of macroscopic phase separation by the long-range repulsive part[5,6,15]. Combinations of density functional theory and a perturbation theory approach, with the clusters modeled for simplicity as spherical, suggest a first-order-like phase transition between the two thermodynamically stable phases, characterized by the discontinuous jump of the cluster size above a critical colloidal density[11,16].

For the calculation of equilibrium (short-time) diffusion and rheological properties in the dispersed-fluid phase such as the hydrodynamic function, $H(q)$, and the high-frequency low-shear viscosity η_∞, we can thus use an easy-to-apply toolbox[17] of well-tested analytic methods where HIs are included, namely a hybrid of the Beenakker-Mazur (BM) and hydrodynamic pairwise additivity (PA) methods[18–21]. This BM-PA hybrid scheme requires $S(q)$ and the radial distribution function, $g(r)$, as the only input. The static input can be calculated, to excellent accuracy for the homogeneous fluid-phase region as we are going to show in comparison with Monte-Carlo (MC) simulation data of $g(r)$, using the thermodynamically self-consistent Zerah-Hansen (ZH) integral equation scheme. This scheme interpolates between the soft mean-spherical closure for small distances of particle pairs and the hypernetted chain closure for large distances[22,23]. For dispersions with a hard-core plus purely repulsive Yukawa potential such as charge-stabilized colloids, the BM-PA hybrid method gives

results in good overall agreement with simulation and experimental data[17,18,24,25]. It can be expected to provide semi-quantitative results for the considered homogeneous SALR systems. Its analytic simplicity makes the BM-PA scheme a convenient tool for assessing general dynamic trends.

The description of the SALR model is given in Sec. 2. In Sec. 3, we discuss the salient features of the static input $S(q)$ and $g(r)$ required for the BM-PA calculations of short-time dynamic properties. Our results for self- and collective diffusion properties, and the sedimentation coefficient of SALR systems are presented in Subsec. 4.1. The high-frequency viscosity, and the performance assessment of two generalized Stokes-Einstein relations, are discussed in Subsec. 4.2. Our conclusions are contained in Sec. 5.

2 Two-Yukawa SALR model

The hard-sphere plus two-Yukawa SALR pair potential $V(r)$ used in our theoretical study of short-time diffusion and rheological properties reads explicitly[26,27],

$$\beta V(x) = \begin{cases} \infty & x < 1 \\ \alpha \left[-K_1 \frac{e^{-z_1(x-1)}}{x} + K_2 \frac{e^{-z_2(x-1)}}{x} \right] & x \geq 1. \end{cases} \quad (1)$$

Here, $x = r/\sigma$ is the inter-particle center-to-center distance, r, in units of the particle diameter σ, and $\beta = 1/(k_B T)$ is the reduced inverse temperature with Boltzmann constant k_B and temperature T. Moreover, z_1 and z_2 determine the range of the attractive and repulsive Yukawa potential parts in units of σ, respectively, and $\overline{K}_1 = \alpha K_1$ and $\overline{K}_2 = \alpha K_2$ are the respective SA and LR reduced potential strengths. To obtain a systematic variation of the potential shape, and to reduce the number of adjustable potential parameters, we follow Costa et al.[14] in demanding that

$$\alpha = -\beta V \left(x = 1^+ \right), \quad (2)$$

which implies that $K_2 = 1 - K_1$. Accordingly, α is identified as the depth of the potential well at two-particle contact in units of $k_B T$. It plays thus the role of an interaction strength parameter equal to the inverse of the reduced effective temperature T^*. In the high-T^* limit for which $\alpha = 0$, the two-Yukawa soft potential contribution in Eq. (1) is negligible, and the particles behave then as hard spheres. Like in Ref.[14], we use the values $K_1 = 1.6306$, $K_2 = 1 - K_1 = 0.6306$, $z_1 = 10$ and $z_2 = 0.5$ describing SALR potential curves of constant effective attraction range, $x_0 = 1.1$, for varying $\alpha > 0$, defined as the distance where $V(x)$ crosses the null line, changing its sign from negative to positive values.

In our study, $\alpha = 1/T^*$ is varied in the interval $[0 - 3]$ so that for the maximal potential depth, $-3k_B T$, particles in contact can still disintegrate by thermal motion. With increasing α, the potential well deepens, and a shallow potential barrier of height $\beta V(x_{max}) \approx 0.36\alpha$ develops at $x_{max} \approx 1.33$, followed for distances $x > x_{max}$ by the monotonic decay of the potential in the range set by $1/z_2$. The second virial coefficient, $B_2^*(\alpha)$, taken in units of the hard-sphere reference value, $(2\pi/3)\sigma^3$, which characterizes the total interaction strength, increases from its value 1 at $\alpha = 0$ to 28 at $\alpha = 3$. Note that with increasing α, the depth of the attractive well and the height of the potential barrier are both enlarged for

fixed ratio, $\overline{K}_1/\overline{K}_2 = 2.59$, of attractive and repulsive soft potential strengths.

The SALR systems discussed in this work are in the particle volume fraction range $0 < \phi \le 0.15$, with values of α selected such that all systems are in the dispersed-fluid state where most particles diffuse individually. There still remains the tendency of clustering as noticed, e.g., by the presence of an IRO low-q peak in $S(q)$.

3 Static properties

Before presenting our results for short-time properties, we discuss first the behavior of the SALR static structure functions $S(q)$ and $g(r)$ constituting the salient input to the dynamic calculations. We employ the thermodynamically self-consistent Zerah-Hansen (ZH) integral equation scheme[23] for calculating the static input which is well suited, and quite accurate, for pair potentials with attractive soft pair potential parts. For simplicity, the potential parameters $\{K_1, K_2, z_1, z_2, \alpha\}$ are held fixed in taking the concentration derivative of the virial pressure needed for the enforcement of thermodynamic self-consistency between the virial pressure and osmotic compressibility thermodynamic routes.

Results for $S(q)$ obtained by the ZH scheme are shown in Fig. 1, for $\phi = 0.1$ and several values of α as indicated. With increasing α, the osmotic compressibility factor, $S(0)$, decreases monotonically. In contrast, the next-neighbor peak of individual particles of height $S(q_m)$ decreases initially slightly for increasing α, taking its minimal value at $\alpha \approx 0.5$ with a subsequent monotonic increase with further increasing α. The peak location, q_m, however, is monotonically increasing. The IRO peak in $S(q)$ becomes first visible for $\alpha \approx 1.5$ at $q_c\sigma \approx 2.5$. It increases with increasing α, while its position q_c is shifted slightly to smaller values. Note that if the attraction strength $\overline{K}_1$ were increased for constant repulsion strength $\overline{K}_2$, the osmotic compressibility is raised instead of being depressed. In completing the discussion of $S(q)$, notice the succession of isosbestic wavenumber points, q_i^{iso}, where the structure factor curves intersect. The α-independent isosbestic points in Fig. 1 can be easily and alternatively identified to good accuracy, in the framework of the simple random phase approximation for $S(q)$, from the roots of the spatial Fourier transform of the soft potential part of $V(x)$, extended into the non-overlap region as $V(x < 1) = 0$.

The here discussed features of $S(q)$ are reflected in the ZH-calculated RDFs shown in Fig. 2 in comparison with our MC simulation data (filled circles). They quantify the growing influence of both the SA and LR potential parts with increasing α, giving rise to a more pronounced microstructure than the one of the hard-core reference system at the same concentration. As it is seen in the main figure part, with increasing α the RDF contact value, $g(x = 1^+)$, grows strongly from 1.3 at $\alpha = 0$ to 28 at $\alpha = 3$, accompanied by the buildup of a pronounced depletion zone inside $1 < x < 2$, and a peak at $x = 2$ of height smaller than one for $\phi = 0.1$ which sharpens and renders larger than one with increasing concentration. The pronounced contact value of $g(r)$ and its adjacent depletion zone reflect primarily the strong influence of the SA, while the peak at $x = 2$ quantifies the enhanced probability, due to the concerted effect of SA and LR, of finding a linear alignment
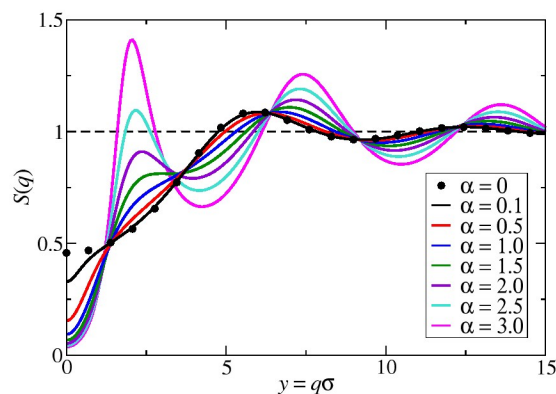

Fig. 1 Zerah-Hansen (ZH) scheme results for the static structure factor, $S(q)$, of the two-Yukawa SALR as a function of reduced wavenumber $y = q\sigma$, for $\phi = 0.1$ and various interaction parameter values α as indicated. The $S(q)$ of the hard-sphere reference system ($\alpha = 0$) is included for comparison (filled black circles).
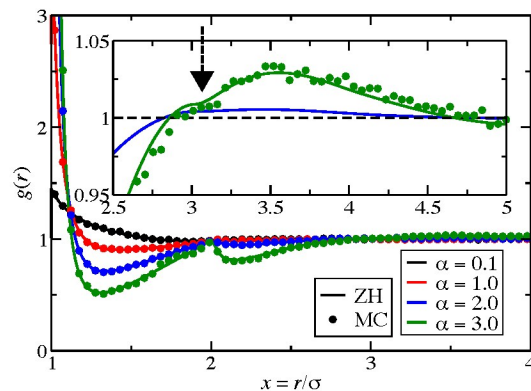

Fig. 2 Radial distribution function, $g(r)$, for $\phi = 0.1$ plotted versus reduced distance $x = r/\sigma$. Solid lines: ZH scheme results. Filled circles: MC simulation data. The inset magnifies the larger-distance region of $g(r)$ for $\alpha = 2$ and 3. The vertical dashed arrow in the inset marks the inflection point visible for $\alpha = 3$ and located at about $2\pi/(q_c\sigma)$.

of two particles with a third one fitting snugly in between (see also [12]). For α values where the IRO-peak has developed, and for pair separations $x \geq 2\pi/y_c = x_c$ where $y_c = q_c\sigma \approx 2.1$, a broad region of $g(x)$ with values weakly enhanced above one is observed (see the inset of Fig. 2) that extends roughly across two particle diameters indicative of the mean transient cluster size [11]. In this larger distance region, $g(x)$ has for $\alpha = 3$ a shallow inflection point at $x_c \approx 3$ marked in the inset by the vertical dashed arrow.

We have used various indicators to make sure that the considered SALR systems belong to the dispersed-fluid phase region: Firstly, according to Fig. 2, the MC simulation calculations of $g(r)$ are in excellent agreement with the ZH scheme results applying to a homogeneous fluid-like system. As a stringent accuracy check, this agreement includes also the contact values $g(\sigma^+)$ for all considered systems. The NVT-ensemble MC simulations have been performed for $N = 4096$ particles in a cubic simulation box, with periodic boundary conditions and pair potential cutoff at $r_{\mathrm{cut}} = 10\sigma$.

Secondly, the IRO peak heights are all well below the critical value $S_{\mathrm{crit}}(q_c) \sim 2.7$, obtained by Godfrin *et al.* [5] as an empirical criterion for the two-Yukawa SALR model signaling in the here considered concentration range a first-order transition from the dispersed-fluid to the cluster-fluid phase. The IRO peak position q_c is shifting to larger values as ϕ is increased (cf. [2]). Thirdly, in the reduced temperature-concentration two-Yukawa SALR phase diagram determined by Godfrin *et al.* (cf. [5]), the state points representing our systems are located above the liquid-liquid phase separation line of the attractive reference system, and well within the dispersed-fluid phase region. In comparison, the cluster-fluid phase is located inside the liquid-liquid phase separation region of the associated Noro-Frenkel reference attractive potential system [5].

For the most concentrated system with $\phi = 0.15$ and $\alpha = 3$, an additional shallow peak in the MC-generated $g(x)$ becomes visible at $x \approx \sqrt{3}$, corresponding to the distance a pair of spheres where an orthogonally aligned dimer of two touching spheres fits snugly in between [12]. Yet, also this system of largest concentration and interaction strength belongs to the dispersed-fluid phase region.

Note that additionally to the ZH-closure employed in the present work, alternative Ornstein-Zernike closure relations have been used for SALR systems that are of comparable accuracy. For example, Costa *et al.* [14] employ the modified hypernetted chain approximation by Rosenfeld and Ashcroft [28], and the self-consistent Bomont-Bretonnet [29,30] closures, respectively. In the context of two-Yukawa potential systems, the importance of thermodynamic self-consistency of the used integral equation scheme is discussed by Kim *et al.* [31].

4 Dynamic properties

For the dispersed-fluid phase, the (colloidal) short-time regime of overdamped Brownian motion is unequivocally given by $\tau_B \ll t \ll \tau_D$, where t is the correlation time. Here, τ_B is the characteristic relaxation time of particle momentum fluctuation correlations which is several orders of magnitude smaller than the characteristic diffusion time, $\tau_D = a^2/d_0$, where d_0 is the single-particle

diffusion coefficient of a monodisperse dispersion [32]. For $t \ll \tau_D$, a Brownian particle has diffused a tiny fraction of its radius a only. This allows for calculating short-time dynamic properties from pure equilibrium averages [32].

Experimentally, the short-time regime can be probed using dynamic light scattering or neutron-spin-echo (NSE) measurements, depending on particle sizes and other characteristics of the system. In both scattering methods, the dynamic structure factor, $S(q,t)$, quantifying spatio-temporal correlations of thermal concentration fluctuations is determined as a function of wavenumber q and correlation time t. The rate of its short-time exponential decay,

$$S(q, t \ll \tau_D) = S(q)\exp\left[-q^2 D(q)t\right], \qquad (3)$$

is characterized by the short-time diffusion function, $D(q)$, which can be expressed by the ratio [18]

$$D(q) = d_0 \frac{H(q)}{S(q)}, \qquad (4)$$

of the hydrodynamic function, $H(q)$, and the static structure factor $S(q) = S(q, t = 0)$. The function $H(q)$ contains information about short-time diffusion processes on colloidal length scales $\sim 1/q$. It an be expressed by an equilibrium average invoking a specific combination of the translational hydrodynamic mobility matrix tensor elements, $\boldsymbol{\mu}_{ij}$, relating the hydrodynamic force on a particle j to the resulting velocity change of a particle i caused by the solvent-mediated HIs. For the hypothetical case of hydrodynamically non-interacting particles, one has $H(q) = 1$, independent of q and concentration ϕ. Any wavenumber dependence of $H(q)$ is a hallmark of the influence of the HIs. The hydrodynamic function can be expressed by the sum,

$$H(q) = H_d(q) + \frac{d_S}{d_0}, \qquad (5)$$

of a wavenumber dependent distinct part, $H_d(q)$, which approaches the value zero for large q, and a self part equal to the short-time self-diffusion coefficient, d_S, expressed in units of d_0. Thus, $H(q \to \infty) = d_S/d_0$. The coefficient d_S quantifies the initial slope of the particle mean-squared displacement in a concentrated dispersion. In the absence of HIs, $H_d(q)$ is identically zero, and d_S reduces to d_0. Theoretically, $H(q)$ can be interpreted as a short-time reduced generalized sedimentation velocity in a homogeneous dispersion subjected to a spatially oscillating weak force field of wavelength $2\pi/q$. Accordingly,

$$K = H(q \to 0) = \frac{V_{\mathrm{sed}}}{V_0} \qquad (6)$$

is the dispersion sedimentation coefficient in a uniform (e.g., buoyancy corrected gravitational) force field, with V_{sed} denoting the mean sedimentation velocity in a concentrated dispersion that reduces to the single-particle sedimentation velocity V_0 at infinite dilution.

Additionally to $H(q)$ characterizing short-time diffusion, as a rheological short-time property of likewise hydrodynamic origin we calculate the high-frequency viscosity, η_∞, which can be measured using a low-amplitude oscillatory shear rheometer operated
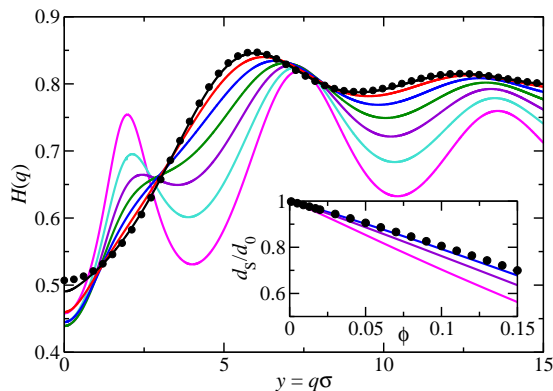
Fig. 3 Hydrodynamic function, $H(q)$, calculated using the BM-PA hybrid method with the structural input presented in Fig. 1, for $\phi = 0.1$ and the same values of α (same color code) as in Fig. 1. Inset: Concentration dependence of the short-time self-diffusion coefficient, d_S/d_0, for various values of α as indicated.

at a frequency large compared to $1/\tau_D$ [33]. In the hypothetical case of a non-dilute dispersion without HIs, η_∞ reduces to the viscosity expression $\eta_0(1 + 2.5\phi)$, including the Einstein intrinsic viscosity contribution for no-slip spheres.

Similarly to earlier theoretical studies of short-time dynamic properties in suspensions with purely repulsive interactions [18], we calculate $H(q)$ using the second-order BM method [19–21] for its wavenumber dependent distinct part, $H_d(q)$, for which the method makes reliable predictions as shown in numerous comparisons with elaborate hydrodynamic force multipoles simulations and experimental data for non-SALR dispersions [18,25]. As regards the calculation of the self-part d_S of $H(q)$, and likewise of η_∞, the PA method [18] is used that accounts for the full two-body HIs part including lubrication effects. The hybrid BM-PA scheme has been successfully applied to hard-sphere and charged-stabilized suspensions, as well as to BSA protein solutions under non-SALR conditions [17,34]. A detailed account of the BM-PA hybrid scheme with numerous applications is given in [18,24], and its extension to particles with internal hydrodynamic structure such as microgels is described in [17]. We merely note here that while the bare PA method with its exact account of two-body lubrication works well for the self-diffusion coefficient and the high-frequency viscosity up to the largest considered concentration $\phi \leq 0.15$, for $\phi \gtrsim 0.08$ it has the tendency to overestimate the q-dependent oscillations in $H_d(q)$. This has been demonstrated for purely repulsive Yukawa systems by the comparison with Stokesian dynamics simulations [35], and a similar trend is observed likewise for SALR systems.

4.1 Diffusion properties and sedimentation coefficient

Results for $H(q)$ obtained by the BM-PA scheme with ZH static structure factor input are shown in Fig. 3, for the same system parameters as in Fig. 1. To our knowledge, this is the first theoretical prediction of a low-q IRO peak in $H(q)$. This peak of $H(q)$

emerges first at larger interaction strengths $\alpha > 1.5$ as the IRO peak of $S(q)$, and in the considered parameter range it does not supersede the next-neighbor peak of $H(q)$. Note that the oscillations in $H(q)$ are triggered by the ones in $S(q)$ which explains why the positions of the IRO and next-neighbor peaks in $H(q)$ are practically coincident with the respective positions, q_c and q_m, of $S(q)$. It is further noticed that the hard-sphere $H(q)$ for $\alpha = 0$ is essentially an upper bound for the curves of $H(q)$ at non-zero α, for wavenumbers located to the right of the IRO peak region. The next-neighbor peak values, $H(q_m)$, are smaller than one which is indicative of a significant influence of the near-distance part of the HIs. In contrast, $H(q_m)$ is larger than one for lower-concentrated systems having purely LR [25].
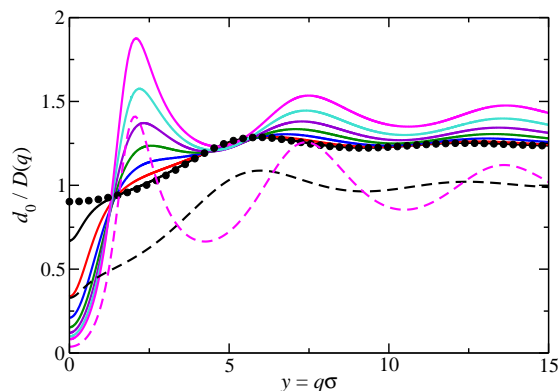

Fig. 4 Inverse, $d_0/D(q)$, of the short-time diffusion function, $D(q)$, in units of the single-particle diffusion coefficient d_0, obtained using the results for $S(q)$ and $H(q)$ in Figs. 1 and 3, respectively. The color code is the same as in Fig. 1. To highlight the strong influence of the HIs, the dashed lines depict $d_0/D(q)|_{no\ HI} = S(q)$ for $\alpha = 0.1$ (black) and $\alpha = 3$ (magenta), respectively, describing hydrodynamically non-interacting particles characterized by $H(q) = 1$.
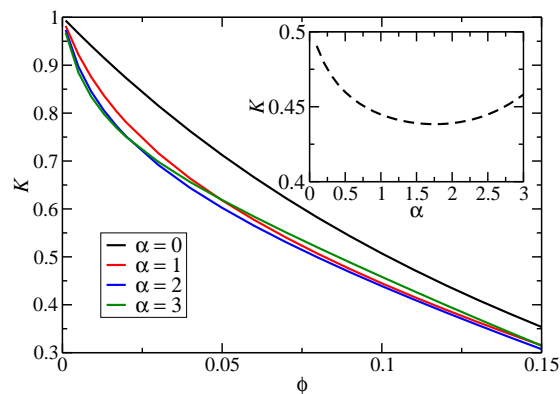

Fig. 5 Concentration dependence of the sedimentation coefficient, $K = V_{sed}/V_0$, for different values of α as indicated. The inset depicts the non-monotonic α dependence of K for $\phi = 0.1$.

The BM-PA scheme supplies also results for the reduced short-time self-diffusion coefficient, $d_S/d_0 = H(q \to \infty)$, depicted in the inset of Fig. Fig. 3. Triggered by the rising RDF contact value with increasing α accompanied by an enhanced transient clustering tendency, d_S decreases monotonically with increasing α and ϕ, taking values below those for hard spheres, namely $d_S(\alpha = 0, \phi)$, at the same concentrations. In fact, transient clustering slows self-diffusion both at short and long times as it has been shown theoretically for sticky hard spheres, and hard spheres with additional square-well attraction [36–38]. While d_S is lowered in systems with enhanced SA having no LR, in systems with pure LR such as in a low-salinity suspension of charge-stabilized particles, the decline of d_S with increasing ϕ is less pronounced than for the hard-sphere reference system, showing typically a fractional $\phi^{4/3}$ concentration dependence [24]. Incidentally, an enhancement of self-diffusion for systems with LR only, and its slowing for systems having solely SA, can be expected both regarding d_S and the long-time self-diffusion coefficient d_L, with $d_L < d_S$, that quantifies the long-time slope of the mean-squared displacement [39]. That d_S decreases with increasing α when the strength both of the SA and LR potential parts are enlarged in proportion to each other is due to the rapid $\mathcal{O}(r^{-4})$ long-distance decay of the hydrodynamic self-mobility tensor associated with d_S [32], putting thus more weight to the near-contact region of $g(r)$. The monotonic decrease of d_S with increasing concentration explains why the α-independent isosbestic points seen in $S(q)$ are absent in $H(q)$. The distinct part $H_d(q)$, however, shares the wavenumber locations, $\{q_i^{iso}\}$, of isosbestic points with $S(q)$, except for the two smallest ones which are not present in $H_d(q)$.

We proceed in discussing the sedimentation coefficient, $K = H(q \to 0)$, whose monotonic decrease with increasing ϕ is shown in Fig. 5. The predicted sedimentation velocity for the considered non-zero α values is smaller than the sedimentation velocity of the corresponding hard-sphere system, i.e. $K(\alpha > 0, \phi) < K(0, \phi)$. This reflects the overall dominant influence of the LR part regarding sedimentation which is known in systems with pure LR to lower the sedimentation velocity [18,24]. The additional influence of the SA part is seen in the, on first sight, surprising non-monotonic α-dependence of K exemplified in the inset of Fig. 5 for $\phi = 0.1$: K decreases for small α and constant ϕ, with a subsequent moderate increase for larger α once it has passed through a minimum at $\alpha \approx 1.8$. The non-monotonic behavior of K as a function of α is a consequence of the delicate interplay of the SA potential part which by its own enhances sedimentation, with the LR part that has the opposite effect. Different from self-diffusion which is most strongly influenced by the near-distance part of the HIs, as a collective property K is also strongly affected by the $\mathcal{O}(r^{-1})$ long-distance part of the HIs. In this context, we refer to a recent multiparticle collisions dynamics (MPCD) simulation study by Moncha-Jorda et al. [40], for the sedimentation coefficient of a dispersion of Brownian particles with short-range interactions only where the SA dominates (i.e., $B_2^* < 0$). In their systems, the slope of the low-ϕ linear form of K changes from negative to positive values when B^* is lowered roughly below -0.87. Due to transient clustering, a non-monotonic ϕ dependence of K is observed for $B_2^* \approx -1.42$. Moncho-Jordá et al. note further that their sys-

tems belong to the homogeneous fluid-phase region such as ours. As a general remark, we note that different from self-diffusion where the long-time coefficient d_L in concentrated systems is substantially smaller than d_S owing to pronounced dynamic caging effects [17], the short-time coefficient K can be expected to be only slightly larger than its long-time counterpart.

Fig. 4 shows the inverse of the diffusion function, $D(q)$, in units of d_0. According to Eq. (3), $D(q)$ can be directly obtained in a dynamic scattering experiment whereas an additional measurement of $S(q)$ is required to determine $H(q)$. The figure highlights the importance of HIs by the comparison with the prediction, $d_0/D(q)|_{no HI} = S(q)$, for hydrodynamically non-interacting particles (dashed lines in Fig. 4) which differs significantly from the result with HIs included. Like for $S(q)$, the IRO peak $d_0/D(q_c)$ for $\alpha = 3.0$ is larger than the next-neighbor peak $d_0/D(q_m)$. Fig. 4 serves further to explain how d_S can be inferred approximately from DLS and NSE experiments where only a finite wavenumber band is accessed. As first suggested by Pusey [41] and theoretically corroborated later by Abade et al. [42], a decent estimate of d_S within a few percent error is given by $D(q)$ evaluated at a wavenumber q^* equal to the first wavenumber situated to the right of q_m where $S(q^*) = 1$. Our results for d_S and $D(q)$ show that this practical way of determining d_S is applicable likewise to SALR systems. However, if $D(q)$ is evaluated instead at a wavenumber q^*, with $S(q^*) = 1$, situated in between the IRO and next-neighbor peaks, d_S is significantly underestimated by about 15%. For a decent estimate of d_S it is thus necessary to cover a sufficiently broad q-range extending beyond the next-neighbor peak region.

4.2 High-frequency viscosity and generalized Stokes-Einstein relations

To arrive at a comprehensive assessment of short-time transport properties of homogeneous SALR systems, we discuss next our predictions for the high-frequency viscosity η_∞. Its concentration dependence is shown in Fig. 6.
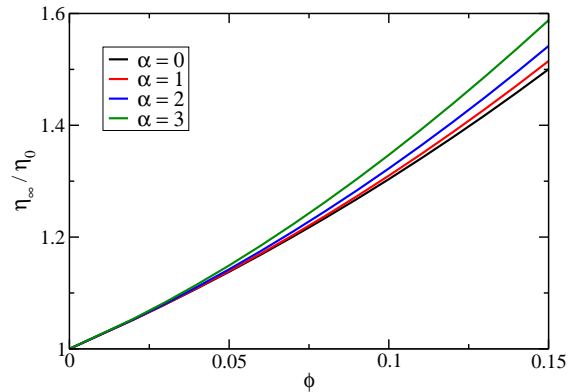

Fig. 6 High-frequency limiting viscosity, $\eta_\infty(\phi)$, in units of the solvent viscosity η_0, as a function of ϕ and for values of α as indicated.

Increasing the concentration implies more pronounced stress relaxation and enhanced viscous dissipation, resulting in an en-

larged viscosity. Furthermore, a monotonic increase of η_∞ above the corresponding hard-sphere result is observed with increasing α. This should be contrasted with a dispersion having LR interactions only, where η_∞ is smaller than in a hard-sphere system of equal concentration[24]. To comprehend this notice that the hydrodynamic shear mobility tensor coupling the hydrodynamic stress dipole acting on a particle surface to the fluid rate-of-strain tensor at the position of another particle is rather short-ranged[43], with an $\mathscr{O}(1/r^6)$ asymptotic decay. The near-contact region of the RDF has thus the strongest influence on the high-frequency viscosity so that with increasing RDF contact value, η_∞ is accordingly increased.

As a useful application we discuss finally for our SALR systems the applicability of two short-time generalized Stokes-Einstein (GSE) relations relating η_∞ to d_S, and to the collective or gradient diffusion coefficient, $d_C = D(q \to 0)$, respectively. Consider the two GSE functions Λ_S and Λ_C defined by

$$\Lambda_S \quad = \quad \frac{\eta_\infty(\phi)}{\eta_0} \frac{d_S(\phi)}{d_0} \qquad (7)$$

$$\Lambda_C \quad = \quad \frac{\eta_\infty(\phi)}{\eta_0} \frac{d_C(\phi)}{d_0} \sqrt{S(q \to 0, \phi)}. \qquad (8)$$

If $\Lambda_S \approx 1$ independent of ϕ and α, then d_S scales with the inverse of η_∞. Likewise, provided that $\Lambda_C \approx 1$ independent of ϕ and α, d_C is proportional to the inverse of the product of η_∞ and the square root of the osmotic compressibility factor $S(0)$. The second GSE relation for d_C has been proposed by Kholodenko and Douglas[44], and it was applied in particular to protein solutions (see, e.g.,[34,45]).
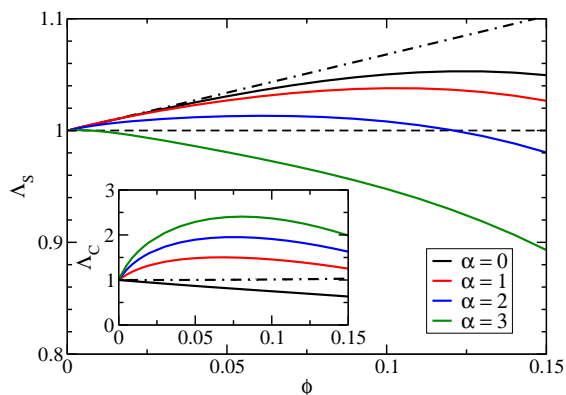

Fig. 7 Self-diffusion GSE function, $\Lambda_S(\phi)$, defined in Eq. (7), for values of α as indicated. Inset: corresponding curves for the Kholodenko-Douglas collective diffusion GSE function $\Lambda_C(\phi)$. The dashed-doted black lines are accurate hard-sphere results ($\alpha = 0$) obtained from the analytic expressions for $d_S(\phi)$ and $\eta_\infty(\phi)$ given in [17].

The approximate validity of these relations would be very useful since η_∞ is then determined more easily by a scattering experiment where smaller amounts of particles are needed than in a rheo-mechanical experiment. Various GSEs have been proposed, and their applicability has been explored theoretically for hard-

sphere and charged-stabilized dispersions[17,18,24]. Our results for $\Lambda_S(\phi)$ and $\Lambda_C(\phi)$ of SALR systems are shown in the main part of Fig. 7, and its inset, respectively, for values of α as indicated. Notice here the different ordinate scales in main figure part and the inset. In the considered ϕ range, the maximal deviation of Λ_S from one is about 10%, showing that the GSE relation for d_S is a useful tool for semi-quantitatively assessing η_∞ in a dynamic scattering experiment. While the Kholodenko-Douglas GSE relation for d_C applies quite well to hard spheres, with $\Lambda_C(\phi)$ being close to one even at $\phi = 0.15$, its applicability worsens significantly with increasing α. Note again the approximate character of the BM-PA scheme, as illustrated in Fig. 7 by the inclusion of the dashed-dotted curves for $\Lambda_S(\alpha = 0, \phi)$ and $\Lambda_C(\alpha = 0, \phi)$, obtained from accurate analytic expressions for the d_S and η_∞ of hard spheres[17]. The deviations of the PA curves for $\alpha = 0$ from these numerically precise GSE functions is due to the underestimation of d_S and η_∞ at larger ϕ by the PA scheme which does not account for hydrodynamic shielding effects associated with non-pairwise additive man-body HIs contributions. The individually smaller errors in d_S and η_∞ introduced by the PA method are propagated by the GSE functions Λ_S and Λ_C as described in Eq. (8).

5 Concluding remarks

In conclusion, our theoretical analysis has shown that the competition of SA and LR leads to unusual features in the concentration and interaction strength dependence of transport properties in the dispersed fluid-phase that are not encountered in systems with either repulsive or attractive soft interactions. An IRO peak signaling clustering tendencies is present also in the hydrodynamic and diffusion functions which grows with increasing interaction strength α. While the self-diffusion coefficient and high-frequency viscosity change monotonically with increasing α, the sedimentation coefficient behaves non-monotonically owing to the subtle interplay of the SA and LR soft potential parts with the short-range and long-range contributions of the HIs. We have analyzed how a decent estimate of d_S in SALR systems is obtained from NSE and DLS experiments performed at a specific wavenumber $q^* > q_m$ with $S(q^*) = 1$, and we have assessed the applicability of two GSE relations for d_S and d_C, respectively. Our general results are helpful as a prerequisite and reference in future studies aimed to identify so far unknown dynamic features, e.g., in the equilibrium cluster phase. Furthermore, the presented work is of relevance to technological applications such as in the modeling of ultrafiltration of protein solutions where diffusion and viscosity properties form key ingredients[46–48]. In future work, we will explore the accuracy of the BM-PA method for systems in the dispersed-fluid phase, and possible extensions of this method to the equilibrium cluster phase, by the comparison with multiparticle collision dynamics simulations. In addition, a comparison of our analytic results with NSE measurements on low-salinity lyzozyme solutions is in progress.

Acknowledgments

Cambridge MA), R.G. Winkler, S. Das, and R. Roa (all FZ Jülich), and M. Heinen (CalTech, Pasadena) for many helpful discussions.

References

1 A. Stradner, H. Sedgwick, F. Cardinaux, W. C. K. Poon, S. U. Egelhaaf and P. Schurtenberger, *Nature*, 2004, **432**, 492–495.

2 F. Cardinaux, E. Zaccarelli, A. Stradner, S. Bucciarelli, B. Farago, S. U. Egelhaaf, F. Sciortino and P. Schurtenberger, *J. Phys. Chem. B*, 2011, **115**, 7227–37.

3 P. D. Godfrin, R. Castañeda Priego, Y. Liu and N. J. Wagner, *J. Chem. Phys.*, 2013, **139**, 154904.

4 Y. Liu, L. Porcar, J. Chen, W. R. Chen, P. Falus, A. Faraone, E. Fratini, K. Hong and P. Baglioni, *J. Phys. Chem. B*, 2011, **115**, 7238–7247.

5 P. D. Godfrin, N. E. Valadez-Pérez, R. Castañeda Priego, N. J. Wagner and Y. Liu, *Soft Matter*, 2014, **10**, –.

6 E. Mani, W. Lechner, W. K. Kegel and P. G. Bolhuis, *Soft Matter*, 2014, **10**, 4479–4486.

7 F. Cardinaux, A. Stradner, P. Schurtenberger, F. Sciortino and E. Zaccarelli, *Europhys. Lett.*, 2007, **77**, 48004.

8 A. J. Chinchalikar, V. K. Aswal, J. Kohlbrecher and A. G. Wagh, *Phys. Rev. E*, 2013, **87**, 062708.

9 R. Piazza, M. Pierno, S. Iacopini, P. Mangione, G. Esposito and V. Bellotti, *Eur. Biophys. J.*, 2006, **35**, 439–445.

10 N. Kovalchuk, V. Starov, P. Langston and N. Hilal, *Adv. Colloid Interface Sci.*, 2009, **147-148**, 144–54.

11 A. Archer and N. Wilding, *Phys. Rev. E*, 2007, **76**, 031501.

12 N. E. Valadez-Pérez, R. Castañeda Priego and Y. Liu, *RSC Adv.*, 2013, **3**, 25110.

13 J.-M. Bomont, J.-L. Bretonnet and D. Costa, *J. Chem. Phys.*, 2010, **132**, 184508.

14 D. Costa, C. Caccamo, J.-M. Bomont and J.-L. Bretonnet, *Mol. Phys.*, 2011, **109**, 2845–2853.

15 J. C. F. Toledano, F. Sciortino and E. Zaccarelli, *Soft Matter*, 2009, **5**, 2390.

16 T. Jiang and J. Wu, *Phys. Rev. E*, 2009, **80**, 021401.

17 J. Riest, T. Eckert, W. Richtering and G. Nägele, *Soft Matter*, 2015, **11**, 2821–2843.

18 M. Heinen, A. J. Banchio and G. Nägele, *J. Chem. Phys.*, 2011, **135**, 154504.

19 C. Beenakker and P. Mazur, *Phys. A Stat. Mech. its Appl.*, 1983, **120**, 388–410.

20 C. Beenakker, *Phys. A Stat. Mech. its Appl.*, 1984, **128**, 48–81.

21 C. Beenakker and P. Mazur, *Phys. A Stat. Mech. its Appl.*, 1984, **126**, 349–370.

22 G. Zerah, *J. Comput. Phys.*, 1985, **61**, 280–285.

23 G. Zerah and J.-P. Hansen, *J. Chem. Phys.*, 1986, **84**, 2336.

24 A. J. Banchio and G. Nägele, *J. Chem. Phys.*, 2008, **128**, 104903.

25 F. Westermeier, B. Fischer, W. Roseker, G. Grübel, G. Nägele and M. Heinen, *J. Chem. Phys.*, 2012, **137**, 114504.

26 S. Kundu, K. Das and V. Aswal, *Chem. Phys. Lett.*, 2013, **578**, 115–119.

27 S. Grobelny, M. Erlkamp, J. Möller, M. Tolan and R. Winter, *J. Chem. Phys.*, 2014, **141**, 22D506.

28 Y. Rosenfeld and N. Ashcroft, *Phys. Rev. A*, 1979, **20**, 1208–1235.

29 J.-M. Bomont and J.-L. Bretonnet, *J. Chem. Phys.*, 2004, **121**, 1548–52.

30 J.-M. Bomont, *J. Chem. Phys.*, 2003, **119**, 11484.

31 J. M. Kim, R. Castañeda Priego, Y. Liu and N. J. Wagner, *J. Chem. Phys.*, 2011, **134**, 064904.

32 G. Nägele, *Phys. Rep.*, 1996, **272**, 215–372.

33 W. B. Russel, *J. Chem. Soc. Faraday Trans. 2*, 1984, **80**, 31.

34 M. Heinen, F. Zanini, F. Roosen-Runge, D. Fedunová, F. Zhang, M. Hennig, T. Seydel, R. Schweins, M. Sztucki, M. Antalík, F. Schreiber and G. Nägele, *Soft Matter*, 2012, **8**, 1404.

35 M. Heinen, P. Holmqvist, A. J. Banchio and G. Nägele, *J. Appl. Crystallogr.*, 2010, **43**, 970–980.

36 B. Cichocki and B. U. Felderhof, *J. Chem. Phys.*, 1990, **93**, 4427.

37 B. Cichocki and B. U. Felderhof, *J. Chem. Phys.*, 1991, **94**, 563.

38 C. Van Den Broeck, *J. Chem. Phys.*, 1985, **82**, 4248.

39 G. Nägele, M. Kollmann, R. Pesché and A. J. Banchio, *Mol. Phys.*, 2002, **100**, 2921–2933.

40 A. Moncho-Jordá, A. A. Louis and J. T. Padding, *Phys. Rev. Lett.*, 2010, **104**, 068301.

41 P. N. Pusey, *J. Phys. A. Math. Gen.*, 1978, **11**, 119–135.

42 G. C. Abade, B. Cichocki, M. L. Ekiel-Jezewska, G. Nägele and E. Wajnryb, *J. Chem. Phys.*, 2010, **132**, 014503.

43 D. J. Jeffrey, *Phys. Fluids A Fluid Dyn.*, 1992, **4**, 16.

44 A. L. Kholodenko and J. F. Douglas, *Phys. Rev. E*, 1995, **51**, 1081–1090.

45 A. Gaigalas, V. Reipa, J. Hubbard, J. Edwards and J. Douglas, *Chem. Eng. Sci.*, 1995, **50**, 1107–1114.

46 R. Roa, E. K. Zholkovskiy and G. Nägele, *Soft Matter*, 2015, **11**, 4106–4122.

47 W. Richard Bowen and P. M. Williams, *Chem. Eng. Sci.*, 2001, **56**, 3083–3099.

48 S. Bhattacharjee, A. S. Kim and M. Elimelech, *J. Colloid Interface Sci.*, 1999, **212**, 81–99.

Unusual dynamic features in dispersions with competing short-range attraction and long-range repulsion

1

deionized protein solution
(Lysozyme)

charged colloids
+ depletant

Dynamics

hydrodynamic function

reduced wavenumber

$y = q\sigma$

- $\alpha = 0$
- $\alpha = 0.1$
- $\alpha = 0.5$
- $\alpha = 1.0$
- $\alpha = 1.5$
- $\alpha = 2.0$
- $\alpha = 2.5$
- $\alpha = 3.0$